catalysts

MDPI

Article

Simultaneous Catalysis of Sulfite Oxidation and Uptake of Heavy Metals by Bifunctional Activated Carbon Fiber in Magnesia Desulfurization

Yuguo Wang, Tieyue Qi, Mengxuan Hu, Yu Yang, Lei Xing and Lidong Wang *

Department of Environmental Science and Engineering, North China Electric Power University, Baoding 071003, China; wangyuguo0315@163.com (Y.W.); qitieyue@hotmail.com (T.Q.); hmx19920514@163.com (M.H.); yangyu2200@126.com (Y.Y.); xingleincepu@hotmail.com (L.X.)

* Correspondence: halburtwang@163.com; Tel.: +86-0312-7525511

Received: 22 December 2019; Accepted: 16 February 2020; Published: 18 February 2020

Abstract: Sulfite and heavy metals are crucial pollutants in the slurry produced by flue gas desulfurization. In this study, a novel cobalt-based activated carbon fiber (Co-ACFs) catalyst-adsorbent was synthesized using an impregnation method; this bifunctional catalyst-adsorbent was used in wet magnesia desulfurization for the simultaneous catalytic oxidation of magnesium sulfite and uptake of heavy metal (Hg^{2+}, Cd^{2+}, and Ni^{2+}) ions. The morphology and surface chemistry of ACFs before and after cobalt loading were investigated using various characterization methods. The kinetics on catalytic oxidation of magnesium sulfite was investigated, and the effects of operation conditions on the simultaneous adsorption capacity of heavy metals were examined. Relative to a non-catalysis material, the 40% Co-ACFs material increased the oxidation rate of magnesium sulfite by more than five times. The Langmuir model can describe the adsorption behavior of Co-ACFs on Hg^{2+}, Cd^{2+}, and Ni^{2+}, indicating that the simultaneous uptake of heavy metals is a single-layer adsorption process. The maximum adsorption capacities for Hg^{2+}, Cd^{2+}, and Ni^{2+} are 333.3, 500, and 52.6 mg/g, respectively. A pseudo-second-order model confirmed that the removal of heavy metals is controlled by the chemisorption process.

Keywords: flue gas desulfurization; cobalt-based catalysis; activated carbon fiber; heavy metal; adsorption

1. Introduction

Flue gas from coal-fired furnaces is a crucial cause of acid rain, haze, and other pollution-related phenomena. The composition of this gas is complex because it contains various pollutants such as dust, SO_2, NO_x, and heavy metals; pollutants have caused serious harm to the atmospheric environment in China [1–4]. However, MgO flue gas desulfurization features high desulfurization efficiency, low energy consumption, less investment requirement, and reliable operation; thus, it satisfies the ultra-low emission requirements of industrial boilers under fluctuating flue gas conditions. Moreover, magnesium sulfate, which is obtained as the desulfurization product, can be used as an industrial raw material or agricultural fertilizer and has a high economic value [5–7]. To prevent the crystallization of magnesium sulfate in the absorption tower in a traditional magnesia desulfurization process, the concentration of magnesium sulfate in the desulfurization solution should be controlled below 10%. Excessive unsaturation (the critical crystallization concentration of $MgSO_4 \cdot 7H_2O$ at 40 °C is approximately 30%) leads to excessive energy consumption in the subsequent evaporation crystallization process, which can limit the wide-scale development of the technology.

The oxidation of magnesium sulfite to magnesium sulfate was proven to be the most economical and effective enrichment method for magnesium sulfate [8]. However, due to the relatively low

oxidation rate of magnesium sulfite, the oxidation is difficult to accomplish in a real desulfurization process. This problem has become the paramount bottleneck of the oxidation enrichment technology. The excessive sulfite might exhaust the dissolved oxygen in the effluent and decomposed into SO_2, resulting in further environmental risks. Meanwhile, a large number of heavy metal particles are collected in the desulfurization slurry, which can migrate and transform during the desulfurization process. For example, Hg^{2+} present in the desulfurized slurry is easily released into the atmospheric environment because the ion is reduced to Hg^0 by sulfite [9–11]. Some co-existing Cd^{2+} ions may co-crystallize with the saturated magnesium sulfate in the recovered products to cause secondary pollution. Therefore, the simultaneous removal of heavy metals from desulfurized slurries becomes another technical problem for magnesium sulfate recovery.

Studies have shown that transition metal ions such as Co^{2+}, Mn^{2+}, Fe^{2+}, and Cu^{2+} can be used for improving the oxidation rate of sulfite. Among these ions, Co^{2+} exhibits the highest performance in terms of sulfite oxidation [12]. However, separating the homogeneous catalyst from the desulfurization slurry is difficult and the material must be supplemented continuously, thus resulting in a high operation cost and secondary pollution due to the use of magnesium sulfate products. To address this problem, our research group developed a series of cobalt-based heterogeneous catalysts [13–18] by using impregnation, coprecipitation, and hydrothermal synthesis. These catalysts effectively solved the catalyst separation problem. However, a magnesium desulfurization slurry that contains heavy metal impurities cannot be treated using conventional alkaline precipitation because a large amount of magnesium would precipitate prior to the heavy metals. If the porous adsorption properties of cobalt-based catalysts can be used to simultaneously remove heavy metals in the catalytic oxidation process of magnesium sulfite, the purity of the magnesium desulfurization by-products can be significantly improved and the secondary pollution of heavy metals can be reduced, which has significant economic and environmental benefits.

Currently, adsorbents used for treating heavy metals in wastewater mainly include porous materials such as activated carbon, carbon nanotubes, metal organic framework (MOF), SBA-15 Silica (SBA, Santa Barbara Amorphous), Calcium Alginate/Graphene and vermiculite-based hydrated zirconia [19–23]. Li et al. [24] synthesized a thiol-functionalized activated carbon material from coal-blended sewage sludge, and the material was found to achieve the highest Brunauer-Emmett-Teller (BET) surface area of 1094 m^2/g when maintained under 500 °C for 30 min. Batch equilibrium tests indicated that the adsorbent had a maximum sorption capacity of 238.1, 96.2, 87.7, and 52.4 mg/g for the removal of Pb (II), Cd (II), Cu (II), and Ni (II) from water, respectively. Narasimha et al. [25] studied the adsorption performance of sulfhydryl carbon nanotubes for the removal of Hg (II). The effects of adsorption time, pH, initial concentration of Hg^{2+}, and carbon nanotube amount on Hg (II) removal efficiency were investigated. The maximum adsorption capacity of Hg^{2+} was 13 mg/g, which is three times more than the capacity of single-walled carbon nanotubes and activated carbon. Wang et al. [26] synthesized sulfonated MOF by using the post-modification method to remove Cd^{2+} from an aqueous solution. The maximum adsorption capacity obtained using isothermal adsorption fitting was 88.7 mg/g, which mainly served as a chelation agent between Cd^{2+} and the $–SO_3H$ functional group. Liu et al. [27] synthesized novel vermiculite-based hydrated zirconia ($ZrO(OH)_2$/VMT) nanocomposites with a specific surface area of 130.86 m^2/g by using a simple ion exchange-precipitation method. The maximum adsorption capacity of Ni^{2+} was 90.21 mg/g.

In recent years, activated carbon fiber (ACF) has attracted widespread attention as a new-generation environment-friendly adsorption/catalyst material. Relative to traditional activated carbon, an ACF material has the advantages of larger specific surface area, higher pore size, more stable performance, faster adsorption rate, and larger adsorption capacity. These advantages cause the ACFs to have a wide application potential in wastewater treatment [28,29]. Yu et al. [30] optimized and improved a nitric acid oxidation process by using microwaves and sonication. The Cu (II) adsorption capacity of ACFs obtained using their microwave-assisted nitric acid oxidation process reached 23.13 mg/g, which was 4.55 times the adsorption capacity of pristine felts. Moreover, the sonication-assisted pickling

regeneration process achieved efficient regeneration and enhancement of Cu (II) adsorptivity for ACFs. Aguilar et al. [31] oxidized ACFs by using ammonium persulfate solution to adsorb Pb (II) present in aqueous solutions. The results revealed that the maximum Pb^{2+} adsorption capacity of modified ACFs was 559 mg/g, which was better than the adsorption capacity of commercial ion exchange resin. Huang et al. [32] modified polyacrylonitrile-based ACF cloths by using nitric acid or by impregnation with a chitosan solution to remove Cu^{2+} from wastewater. Experimental results revealed that the maximum Cu^{2+} electrosorption capacity of chitosan-impregnated ACF cloths was 0.854 mmol/g, which was approximately 2.2 times higher than the capacity of pristine cloths. Moreover, ACFs also showed unique performance characteristics in industrial catalysis. Lin et al. [33] successfully prepared CF@CNF by one-step carbonizing CF-embedded PAN electrospun fiber to activate peroxymonosulfate (PMS)for generating sulfate radicals and then decolorize amaranth in water. Beswick et al. [34] reported high performance of Fe-oxide NPs supported on activated carbon fibers (ACFs) to reduce different functionalized nitroarenes. Hung [35] synthesized Cu-ACFs by wet impregnation method to oxidize ammonia solution. However, little information is available on the catalysis performance of modified ACFs on sulfite oxidation. Its properties of simultaneous uptake of heavy metals is yet unknown although it can serve as a promising adsorbent for the wet desulfurization.

In this study, the cobalt-based ACFs, Co-ACFs, were synthesized using the impregnation method, which were characterized using N_2 adsorption–desorption, X-ray photoelectron spectroscopy (XPS), scanning electron microscopy (SEM), transmission electron microscopy with energy dispersive spectrometer (TEM-EDS), fourier-transform infrared spectroscopy (FT-IR)and Boehm titration. The kinetics of magnesium sulfite oxidation in presence of Co-ACFs were investigated. The performance of the fibers in simultaneously enhancing the oxidation rate of $MgSO_3$ and removing heavy metal ions (Hg^{2+}, Cd^{2+}, and Ni^{2+}) was investigated. The Hg^{2+}, Cd^{2+}, and Ni^{2+} adsorption properties in a single-component simulated desulfurization slurry were studied. Moreover, the kinetics and isothermal adsorption characteristics of Co-ACFs for Hg^{2+}, Cd^{2+}, and Ni^{2+} were discussed. The mechanism of the adsorption reaction was revealed. These results provide useful reference information for the recovery of by-products and the simultaneous removal of multiple pollutants in the wet-desulfurization process.

2. Results and Discussion

2.1. Characterization of ACFs

2.1.1. SEM

Figure 1a–c shows the appearance of ACFs after acid pickling, which is maintained as a continuous and smooth fiber. However, the surface of the Co-ACFs become relatively rough after the introduction of cobalt species. Figure 1d implies that some fibers are broken because the Co-ACFs catalyst-adsorbent has been treated at 350 °C. According to Figure 1f, a number of small convex particles are observed on the surface of ACFs, which might be ascribed to the deposit of cobalt oxide.

TEM-EDS characterization was further conducted to investigate the existence of cobalt oxide particles and the cobalt content in Co-ACFs. Figure 1g shows that Co-ACFs exhibits a fiber-shaped structure being adhered with spherical dots. These spherical dots are ascribed to the cobalt oxide particles. Besides, the cobalt content is calculated to be 33.93% according to the peak area of Co in Figure 1i, which is closed to the nominal cobalt loading (40%).

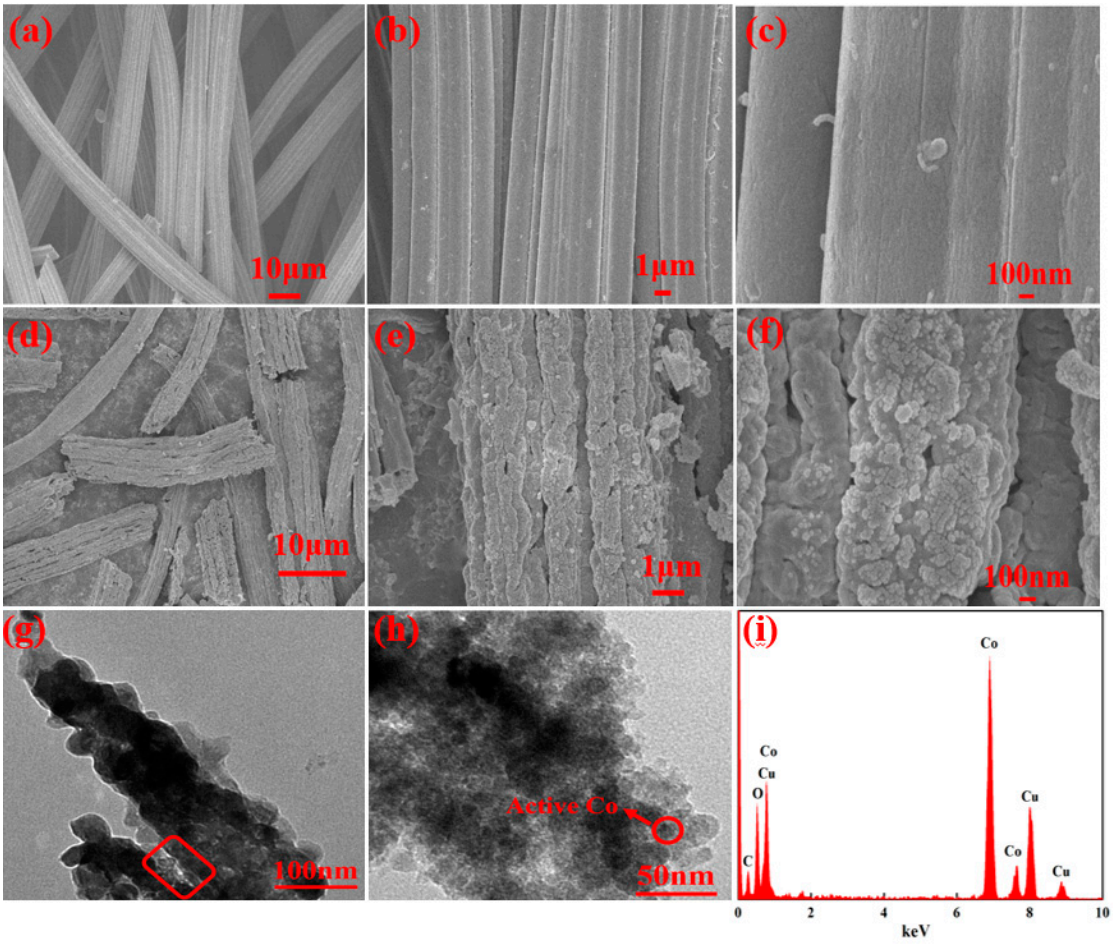

Figure 1. SEM images of (**a**, **b**, **c**) ACFs after acid treatment; (**d**, **e**, **f**) 40% Co-ACFs and (**g**, **h**) TEM image and (**i**) EDS pattern of 40% Co-ACFs.

2.1.2. N_2 Adsorption-Desorption

As depicted in Figure 2, all adsorption isotherms are Langmuir IV isotherms with a typical H4 hysteresis loop. This finding indicates that the samples maintain their original highly ordered mesoporous structures even after Co-based modification. The adsorption capacity of Langmuir IV isotherm is low at low relative pressures. The adsorption capacity increases greatly as P/P_0 increased, thus indicating that a few micropores exist in ACFs and Co-ACFs. Due to the introduction of Co-based active sites, the specific surface area and pore volume decrease from 1035 to 780 m^2/g and 0.57 to 0.42 cm^3/g, respectively. Moreover, the average pore diameter increases from 2.102 to 3.312 nm. The reason for these changes may be that the cobalt oxide particles adhere to the surface of ACFs or fill the gaps between the channels, thus resulting in a decrease in the specific surface area and pore volume. The average pore diameter slightly increases with the introduction of the cobalt oxide particles because the inner walls of the channels may be destroyed by nitric acid impregnation. The pore volume distributions could be seen in Figure 2c,d, and the physical properties of the catalysts are displayed in Table 1. Based on the shape of hysteresis loop in Figure 2c,d, it can be seen that the two materials have a narrow and uniform pore. Overall, the specific surface area, pore size, and size of the ACFs are only limitedly decreased after the loading of cobalt, indicating that cobalt impregnation does not impact the structure of the ACFs support.

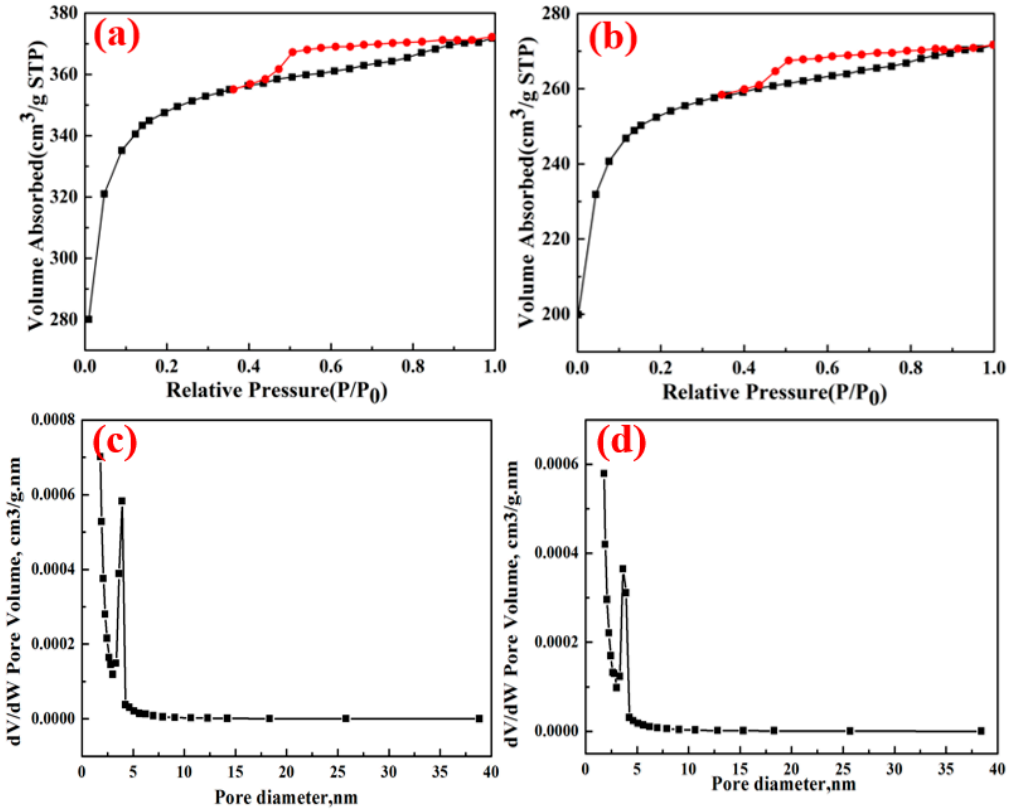

Figure 2. N_2 adsorption−desorption isotherms (**a**) ACFs and (**b**) 40% Co-ACFs, red line: adsorption curve, black line: desorption curve; pore size distributions (**c**) ACFs and (**d**) 40% Co-ACFs.

Table 1. Physical properties of Co loading catalysts.

Sample	Specific Surface Area, $m^2 \cdot g^{-1}$	Pore Volume, $cm^3 \cdot g^{-1}$	Average Pore Size, nm
ACFs	1035	0.57	2.102
40% Co-ACFs	780	0.42	3.312

2.1.3. FT-IR

FT-IR is a powerful tool for revealing the information of functional groups on an adsorbent surface. From Figure 3, the ACFs sample possesses abundant surficial –OH group with the stretching vibration at approximately 3450 cm^{-1}, agreeing well with the previous reports [30]. In contrast, the intensity of the feature peak of –OH group from the Co-ACFs support is weakened obviously. It may be caused by decomposition of –OH group during calcination of the catalyst at 350 °C. The absorption bands at 2900, 1740, 1600, 1400, and 1200–1000 cm^{-1} correspond to the absorption peaks of $–CH_2$ [36], lactone, aromatic ring or carbonyl [37], COO^- or aromatic ring C=C, and phenol C–O or –OH [38]. This indicates that the impregnated cobalt does not substantially affect the number of oxygen-containing functional groups, which is in good agreement with the results of Boehm titration.

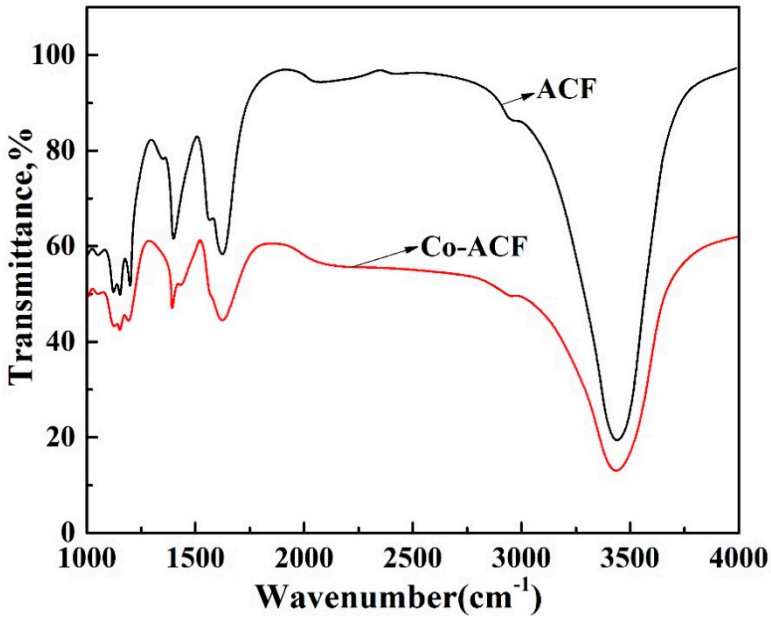

Figure 3. FT-IR spectra of ACFs and 40% Co-ACFs.

2.1.4. XPS Pattern

Co 2p XPS of the Co-ACFs catalyst-adsorbent is presented in Figure S1. The peaks centered at 780.0 and 796.1 eV are correspond to Co $2p_{3/2}$ and Co $2p_{1/2}$, respectively. The Co $2p_{3/2}$ could be further fitted into two bands centered at 779.8 and 781.5 eV, which are assigned to the Co^{2+} and Co^{3+} species, respectively [39]. The peak at 786.2 eV is attributed to the shakeup satellites of Co^{2+} and Co^{3+} species [40–42]. The Co^{2+} and Co^{3+} species might be derived from the Co_3O_4 on ACFs, agreeing well with Sexton et al. [43,44]

2.1.5. Boehm Titration

The results of Boehm titration are listed in Table 2. The number of acid groups increases significantly after ACFs being pretreated with nitric acid, thus resulting in an increase in the number of negative charges on the carbon surface. This increase can provide more lone pair electrons for heavy metal ions and enhance the adsorption performance of the materials. The amount of cobalt loading has a slight effect on the acid group content, thus indicating that the amount of cobalt loading had a slight effect on the removal efficiency of ACFs. Acidic oxygen-containing functional groups polarizes ACFs. According to the principle of similar compatibility, modified ACFs can effectively adsorb various polar compounds.

Table 2. Content of oxygen functional groups on ACFs surface before and after cobalt loading.

Material	Acidic Group (mmoL/g)
Untreated ACFs	0.7861
0%Co-ACFs	2.4903
10%Co-ACFs	2.5010
20%Co-ACFs	2.5443
30%Co-ACFs	2.5809
40%Co-ACFs	2.5909

2.2. *Catalytic Performance Measurement*

The catalytic performance of Co-ACFs with dissimilar Co loading levels (10, 20, 30, 40, and 50 wt. %) in the oxidation of $MgSO_3$ are investigated. In Figure 4a, a gradual increase of the oxidation

rate is observed with increasing Co loading levels from 10% to 40%. It is due to the substantial catalysis activity of Co distributing equally on the surface of ACFs. However, the tendency declines slightly after Co loading reaches 50 wt. %, which might be due to the fact that the excessive Co species has agglomerated on the surface of support [13,14,16,45,46]. Moreover, the catalysis performance of cobalt-based catalysts for sulfite oxidation, including Co-MS, Co-CNTs, Co-SBA-15, and Co-TiO_2, are thoroughly compared in Figure S3, in which the active cobalt species are loaded onto the different supports. It shows that 40% Co-ACFs dominates the catalytic performance at the same concentration of 0.5 g/L, which can serve as a promising candidate for the real applications.

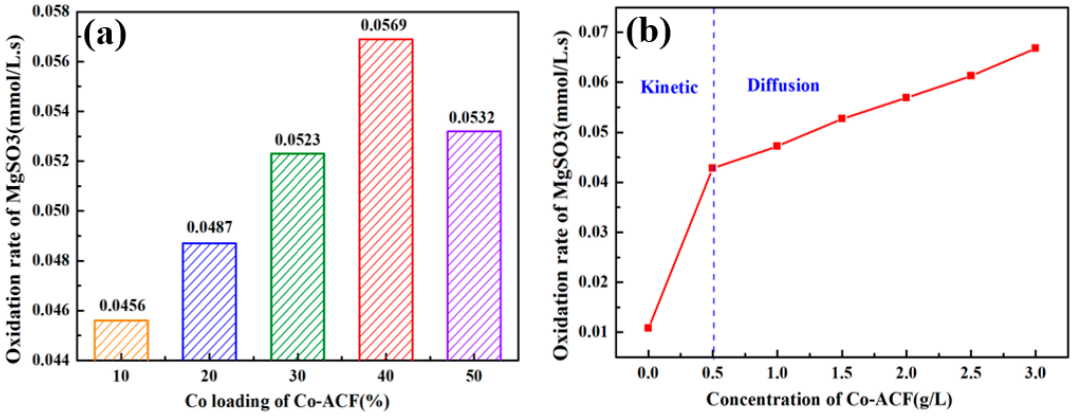

Figure 4. (**a**) Effect of impregnated Co on oxidation rate of $MgSO_3$; (**b**) Effect of catalyst concentration on the oxidation rate of $MgSO_3$ (Co wt % = 40%).

Figure 4b shows the effect of Co-ACFs concentration on the oxidation of $MgSO_3$. The oxidation rate is found increase sharply with the catalyst concentration increasing from 0 to 0.5g/L, suggesting that the overall oxidation rate is controlled by the chemical reaction between the oxygen and sulfite. However, the increasing tendency of oxidation rate become flattened when the catalyst concentration approached higher than 0.5g/L, implying that the overall oxidation is controlled by both the chemical reaction and the diffusion of reactants. These findings are consistent with the results reported by Sathyamurthy [47].

2.3. Simultaneous Removal of SO_3^{2-} and Heavy Metal Ions

Figure 5 reveals that the presence of heavy metal ions slightly inhibits the oxidation of magnesium sulfite. The inhibition intensity is in the following order: $Ni^{2+} > Hg^{2+} > Cd^{2+}$. This may be due to the fact that a portion of the active cobalt is covered after Hg^{2+}, Cd^{2+}, and Ni^{2+} adsorbed on the ACFs surfaces, which hinders the oxidation of magnesium sulfite to some extent. However, the catalytic oxidation rate of $MgSO_3$ is approach five times the noncatalytic rate in the presence of heavy metal ions, thus indicating that heavy metal ions do not contribute any obvious toxicity to the oxidation of SO_3^{2-} in the typical magnesium desulfurization slurry. Figure 5b reveals that the removal efficiency of Co-ACFs for Hg^{2+}, Cd^{2+}, and Ni^{2+} is higher in the absence of sulfite than in the presence of sulfite. The removal efficiency of Hg^{2+}, Cd^{2+}, and Ni^{2+} decrease by 3.6%, 7.3%, and 1.3%, respectively, in the presence of sulfite. However, the removal efficiency of the three heavy metal ions remains above 90%, thus indicating that Co-ACFs has a high adsorption performance for heavy metals and SO_3^{2-} does not significantly inhibit the adsorption progress.

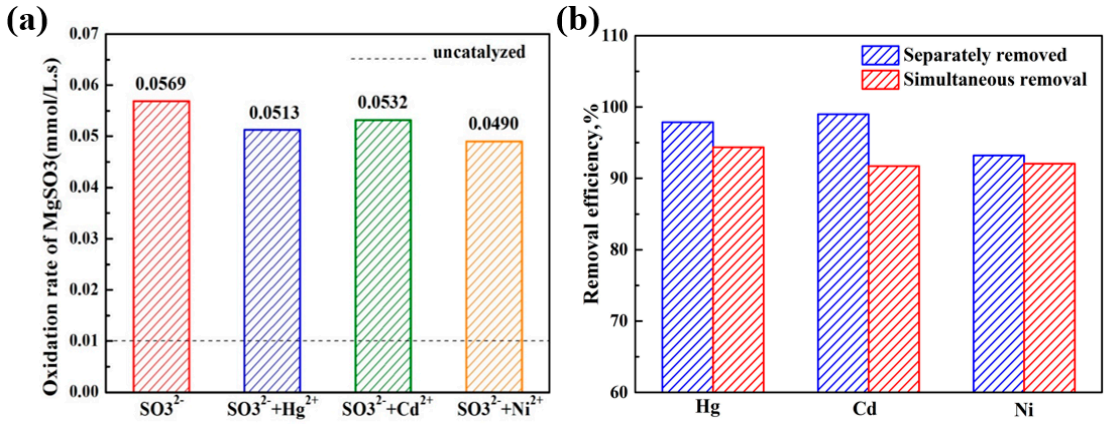

Figure 5. Simultaneous removal of Hg^{2+}, Cd^{2+}, Ni^{2+}, and $SO_3{}^{2-}$ (Co wt % = 40%). (**a**) Effect of heavy metal ions on the oxidation rate of $MgSO_3$. (**b**) Effect of $SO_3{}^{2-}$ on the removal efficiency of heavy metal ions.

2.4. Adsorption Properties of Co-ACFs for Hg^{2+}, Cd^{2+}, and Ni^{2+}

2.4.1. Effect of Cobalt Loading

The removal efficiency of ACFs after cobalt loading is higher than pure ACF for Hg^{2+}, Cd^{2+}, and Ni^{2+}, as presented in Figure 6. It might be owed to the deposit of cobalt oxide on the surface of ACFs, which has been heated for 4h at 350 °C. As a result, the appearance becomes rather rough, favoring to adsorbing the heavy metals efficiently. This finding is in good agreement with the SEM results in Figure 1. The removal efficiency gradually increases with the increase of cobalt loading in the ACFs from 0 to 40 wt. %. When the loading of cobalt reaches 40%, the removal efficiency of Hg^{2+}, Cd^{2+}, and Ni^{2+} reach 95%, 90%, and 85%, respectively, thus revealing high adsorption performance. The BET surface area of the Co-ACFs significantly decreases with increase in cobalt loading, thus indicating that the adsorption of heavy metals is not mainly dependent on the BET surface area of the ACFs. In addition, according to the Boehm titration in Table 2, oxygen-containing functional groups are slightly increased after inducing of cobalt into ACFs, which might benefit for removal of the heavy metals.

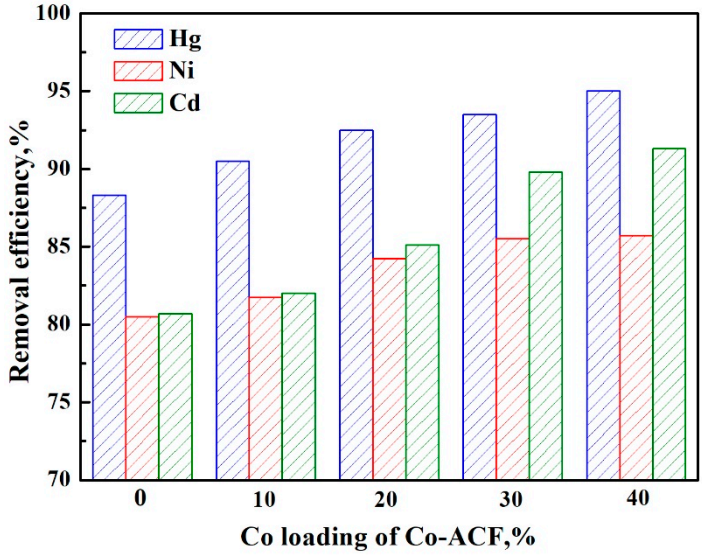

Figure 6. Effect of Co loading on the removal efficiency of Hg^{2+}, Cd^{2+}, and Ni^{2+}.

2.4.2. Effect of Adsorption Time

The effect of the adsorption time on the removal efficiency of Co-ACFs is investigated when the initial concentrations of Hg^{2+}, Cd^{2+}, and Ni^{2+} are 2, 2, and 10 mg/L, respectively. Figure 7a presents that the removal efficiency of the three heavy metals increases rapidly in the first 10 min and attains a value higher than 70%. The adsorption capacity of Co-ACFs for Hg^{2+} and Cd^{2+} exceed 80%, and then, the adsorption process become approximately invariable after 60 min. This phenomenon may have been caused by the high concentrations of Hg^{2+}, Cd^{2+}, and Ni^{2+} in the solution at the initial adsorption stage. A large number of vacant surface sites is probably available for adsorption. The repulsive force forms simultaneously by the surface of the catalyst-adsorbent and the heavy metals in the solution may have caused the gradual equilibrium of the adsorption process. The excellent performance of the catalyst-adsorbent Co-ACFs in the experiment can meet the requirements of industrial wastewater discharge.

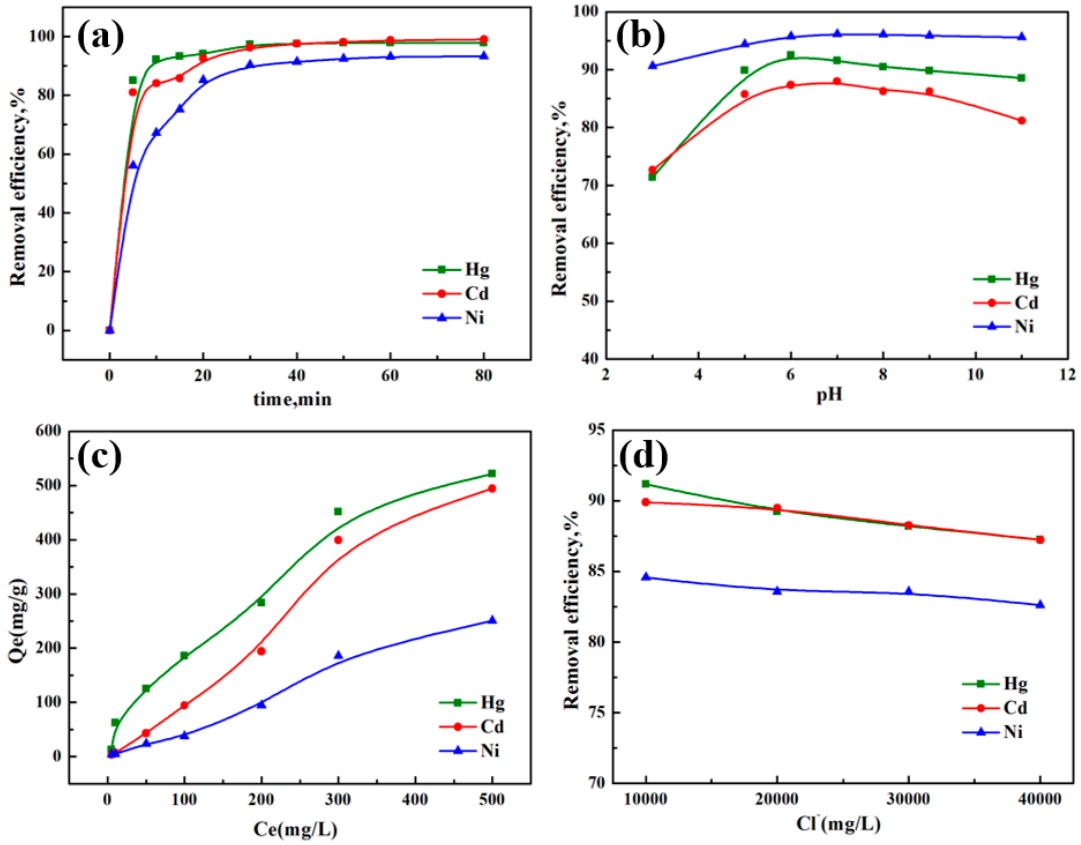

Figure 7. Parametric tests of the adsorption of heavy metals under the optimized dosage levels of Co-ACFs (Co wt % = 40%). (**a**) Effect of adsorption time; (**b**) Effect of pH; (**c**) Effect of the initial concentration of heavy metal ions in the solution; (**d**) Effect of Cl^- concentration.

2.4.3. Effect of pH

Solution pH is a crucial parameter that affects adsorption behavior [48,49] because it not only affects the charge distribution and electrical properties on the surface of ACFs but also determines the binding site between metal ions and catalyst-adsorbent. Thus, the pH of a solution affects the removal efficiency of heavy metal ions. As shown in Figure 7b, the removal efficiency of heavy metal ions is initially increased but then decreased slightly as the pH value of the solution is increased. The removal efficiency peaks at pH 5–7. This range of pH values represents acidic conditions and thus is not conducive to the adsorption of Hg^{2+} and Cd^{2+}. The removal efficiency of Hg^{2+} and Cd^{2+} is only 72% at pH 3. The removal efficiency of Hg^{2+} is higher than 90% when the pH value increases from

5 to 6. The Hg^{2+} removal efficiency decreases slightly with further increase in the pH value. This decrease may have been caused by the mercury ions that mainly exist in the form of Hg^{2+} under an acidic environment. The H^+ ions in the solution might compete with the positively charged Hg^{2+} ions for the active sites on the surface, thus resulting in a low adsorption efficiency. With further increases in the pH value, the concentration of H^+ decreases and the competition between H^+ and metal ions decreases. This causes the removal efficiency to increase rapidly. The dominant Hg (II) species is $Hg(OH)_2$ [48] at a high pH value; thus, the pH value should be strictly controlled during the adsorption process. The Cd^{2+} adsorption tendency of Co-ACFs is similar to the Hg^{2+} adsorption tendency, and the change in the pH value has no significant effect on the removal efficiency of Ni^{2+}. In a typical magnesia-based desulfurization process, the pH value of the desulfurization slurry ranged from 5 to 6. The experimental results prove that the removal efficiency of Hg^{2+}, Cd^{2+}, and Ni^{2+} is more than 80% for pH values between 5 and 6. Co-ACFs delivers excellent adsorption performance under these conditions, which are typical of desulfurization slurry; thus, Co-ACFs materials can meet the requirements of wastewater desulfurization treatment.

2.4.4. Effect of the Initial Concentration of Hg^{2+}, Cd^{2+}, and Ni^{2+} in the Solution

Figure 7c displays that the equilibrium adsorption capacity increased with increases in the equilibrium concentrations of Hg^{2+}, Cd^{2+}, and Ni^{2+}. When the equilibrium ion concentration ranges from 0 to 300 mg/L, the adsorption capacity increases rapidly. The increase rates of Hg^{2+} and Cd^{2+} are much higher than that of Ni^{2+}. Subsequently, the increasing tendency flattens. The maximum adsorption capacities of Co-ACFs for Hg^{2+}, Cd^{2+}, and Ni^{2+} are 333.3, 500, and 52.6 mg/g, respectively, according to the adsorption isotherm fitting. As shown in Table S1, in contrast to other porous materials, the bifunctional catalyst-adsorbent Co-ACFs has a higher adsorption capacity for uptake of heavy metals. Especially, modification with nitric-acid treatment increases the oxygen-containing functional groups on the surface of ACFs. These groups can markedly increase the amount of negative charges on the carbon surface, thus enhancing the adsorption performance for heavy metals. Therefore, Co-ACFs can be a promising bifunctional catalyst-adsorbent for the removal of heavy metals from aqueous solution in practical application.

2.4.5. Effect of Cl^- Concentration

Typical desulfurization wastewater contains staggering levels of chloride. Moreover, the concentration of Cl^- is generally in the range of 8000–20,000 mg/L, which may have some influence on the adsorption of heavy metal ions. Thus, the adsorption efficiency of Co-ACFs for Hg^{2+}, Cd^{2+}, and Ni^{2+} is measured under different Cl^- concentrations. The results presented in Figure 7d reveals that the removal efficiency of heavy metal ions decreases slightly with increase in the Cl^- concentration. Among these heavy metal ion adsorption phenomena, the adsorption of Hg^{2+} in the solution has the largest effect. This effect may have been caused by the formation of Hg-Cl complexes in the presence of compounds of Cl^-; these products include $HgCl_2$, $HgCl_3^-$, and $HgCl_4^{2-}$. Thus, the adsorption of Hg^{2+} is inhibited by Co-ACFs. Cd^{2+} exists in the form of cadmium chloride colloid when a large amount of Cl^- is in the desulfurizing slurry; this also affects the removal efficiency of Cd^{2+} by Co-ACFs. The concentration of Cl^- has almost no effect on the removal efficiency of Ni^{2+}.

2.5. Adsorption Mechanism

2.5.1. Adsorption Isotherms

Figure 8 and Table 3 reveal that the Langmuir model (R^2 = 0.905, 0.970, and 0.967) describes the adsorption behavior of Hg^{2+}, Cd^{2+}, and Ni^{2+} on the Co-ACFs more accurately than the Freundlich model, thus indicating that the adsorption on Co-ACFs can be regarded as a monolayer adsorption process. According to the Langmuir model, the maximum adsorption capacities are 333.3, 500, and 52.6 mg/g for Hg^{2+}, Cd^{2+}, and Ni^{2+}. These values are similar to the experimental data values. Moreover,

the empirical constant *n* of the Freundlich equation is greater than 1 for all heavy metal ions, thus indicating that the Co-ACFs adsorbs Hg^{2+}, Cd^{2+}, and Ni^{2+} easily.

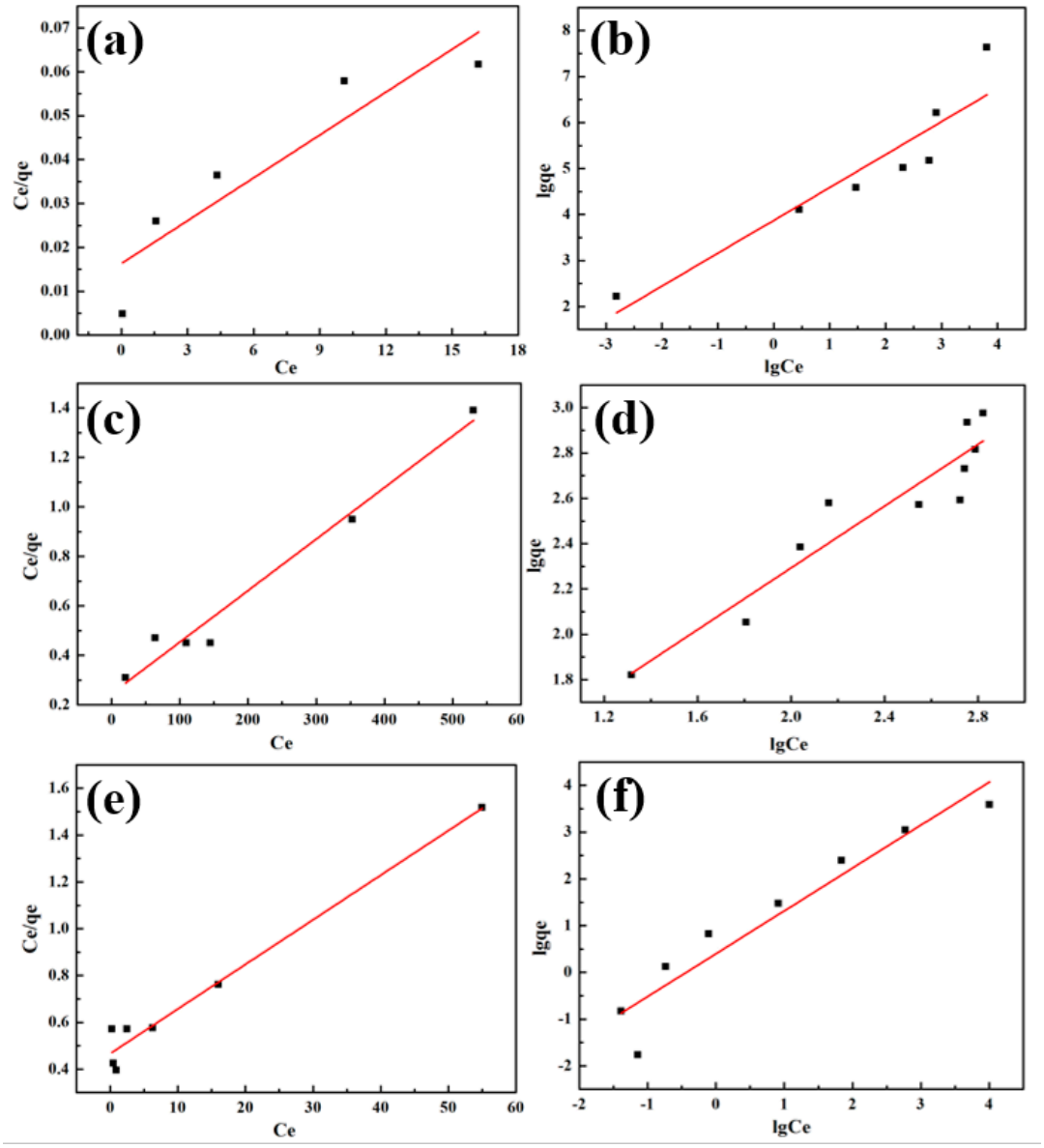

Figure 8. Adsorption isotherms model (Co wt % = 40%). (**a**, **c**, **e**) Langmuir isotherm for Hg^{2+}, Cd^{2+}, and Ni^{2+}; (**b**, **d**, **f**) Freundlich isotherm for Hg^{2+}, Cd^{2+}, and Ni^{2+}.

Table 3. Adsorption isotherm parameters.

Metals	Langmuir			Freundlich		
	K_L	Q_m	R^2	K_F	n	R^2
Hg^{2+}	6.25	333.3	0.905	55.92	6.25	0.851
Cd^{2+}	3.98	500.0	0.970	1.22	8.40	0.881
Ni^{2+}	2.14	52.6	0.967	1.49	1.39	0.902

2.5.2. Adsorption Kinetics

Adsorption kinetics in Figure 9 can provide information pertaining to the adsorption rate and reaction pathway and thus adsorption kinetics parameters are considered to be key factors in the

evaluation of adsorption mechanisms. A comparison of the values of the coefficient of determination R^2 listed in Table 4 reveals that the correlation coefficients of Hg^{2+}, Cd^{2+}, and Ni^{2+} are 0.999, 0.998, and 0.999, respectively, for the pseudo-second-order kinetic model, which is higher than those determined by the pseudo-first-order linear correlation coefficients of 0.774, 0.743, and 0.947. The theoretical q_e values obtained from the pseudo-second-order kinetic model are 4.00, 5.32, and 9.34 mg/g for Hg^{2+}, Cd^{2+}, and Ni^{2+}, respectively, which is similar to the experimental data. These results suggest that the adsorption of Co-ACFs follows pseudo-second-order kinetics, thus implying that the adsorption process is controlled by chemical adsorption.

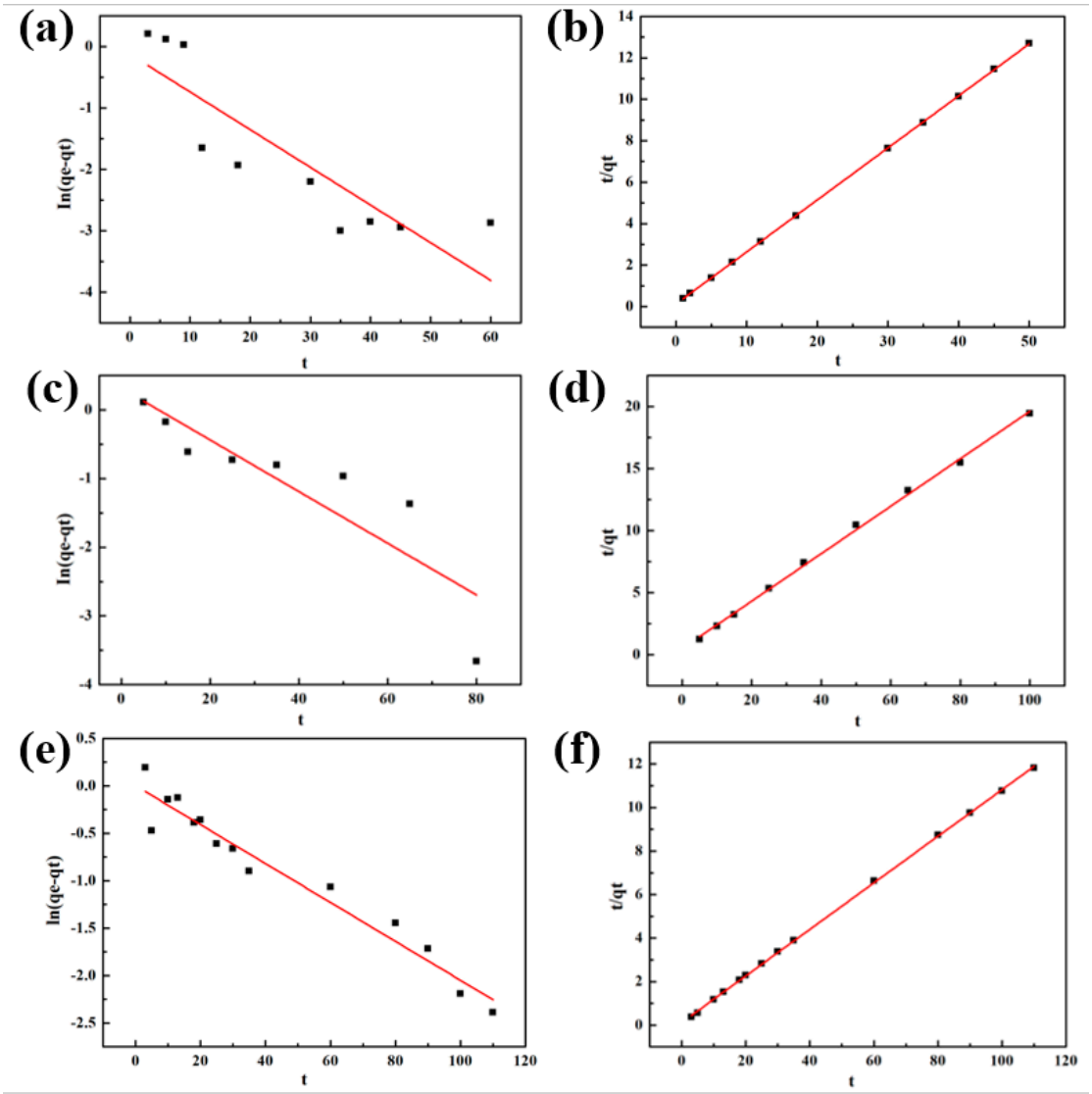

Figure 9. Adsorption kinetics model (Co wt % = 40%). (**a**, **c**, **e**) pseudo-first-order model (Hg^{2+}, Cd^{2+}, Ni^{2+}); (**b**, **d**, **f**) pseudo-second-order model (Hg^{2+}, Cd^{2+}, Ni^{2+}).

Table 4. Adsorption kinetic parameters.

Metals	Pseudo-first-order Model			Pseudo-second-order		
	k_1	q_e	R^2	k_2	q_e	R^2
Hg^{2+}	0.06	1.005	0.774	0.46	4.00	0.999
Cd^{2+}	0.035	1.361	0.743	0.07	5.32	0.998
Ni^{2+}	0.02	1.010	0.947	0.09	9.34	0.999

3. Materials and Methods

3.1. Chemicals

The ACFs material used in this study was purchased from the Shanghai Tianxiang Textile Technology Co., Ltd (Shanghai, China). A standard mercury solution was purchased from the National Center of Analysis and Testing for Nonferrous Metals and Electronic Materials (Beijing, China). Hydrochloric and nitric acids were superior pure reagents. The samples of barium chloride, magnesium chloride, sodium sulfite, cobalt nitrate, nickel nitrate, cadmium chloride, and sodium hydroxide were of analytical grade and were purchased from Huaxin Reagent Co., Ltd (Baoding, China).

3.2. Co-ACFs Catalyst-Adsorbent Synthesis

The purchased ACFs cloth was cut into squares of 1 cm × 1 cm and soaked in 50 vol % HNO_3 for 5 h, which can increase the oxygen-containing functional groups on the surface of ACFs for adsorbing the heavy metals. Hereafter, the ACFs sample was washed until it reached a neutral pH value and dried at 80 °C for 6 h. Moreover, 2 g of pretreated ACFs were immersed in 200 mL $Co(NO_3)_2{\cdot}6H_2O$ solution at a stirring rate of 180 rpm at 25 °C for 6 h. According to Equation (1), the expected stoichiometry of cobalt nitrates corresponding to the nominal cobalt loading of 10 wt. %, 20 wt. %, 30 wt. %, 40 wt. %, and 50 wt. %, when the mass of ACFs is 2.0 g, are 0.986 g, 1.973 g, 2.959 g, 3.946 g and 4.932 g, respectively. The products were dried for 12 h at 80 °C and then roasted in a tube furnace fluxed with N_2. During the roasting process, the temperature was increased to 80 °C in 1 h and then maintained at 80 °C for another 1 h. Subsequently, the temperature was further increased to 350 °C and then maintained at 350 °C for another 4 h. Then, Co-ACFs material was obtained by natural cooling to room temperature.

$$\begin{aligned} \text{Nominal Co loading} &= \frac{m_{Co}}{m_{support}} \times 100\% \\ &= \frac{m_{Co(NO3)2{\cdot}6H2O}}{m_{ACF}} \times \frac{M_{Co}}{M_{Co(NO3)2{\cdot}6H2O}} \times 100\% \end{aligned} \quad (1)$$

where the m_{Co} denotes the mass of Co element; $m_{support}$ represents the mass of support; the $m_{Co(NO3)2{\cdot}6H2O}$ is the mass of $Co(NO_3)_2{\cdot}6H_2O$; m_{ACF} represents the mass of ACF; M_{Co} is the relative atomic mass of Co; $M_{Co(NO3)2{\cdot}6H2O}$ is the molecular weight of $Co(NO_3)_2{\cdot}6H_2O$.

3.3. Catalyst-Adsorbent Characterization

A scanning electron microscope (S4800, Hitachi, Japan) was used to observe the surface morphology and distribution of cobalt particles of the ACFs and Co-ACFs samples. A transmission electron microscope (TEM; JEM-2100, JEOL, Japan) at 200 kV was paired with an energy dispersive spectrometer (EDS) at 15–20 kV to observe the crystallization structure of the sample and perform a surface element analysis. The N_2 adsorption–desorption isotherm of ACFs before and after Co loading was determined by a surface area and porosity analyzer (Tristar II 3020, Micromeritics Instrument Corporation, Norcross, G.A., USA). The specific surface area and pore size distribution of the catalyst were calculated using the BET equation and Barrett-Joyner-Halenda (BJH) method, respectively. X-ray photoelectron spectroscopy (XPS; ESCALAB 250, Waltham, G.A., USA) was applied to analyze the surface elemental composition and valence of the Co-ACFs. The functional groups on the surface of the ACFs and the Co-ACFs adsorbed with heavy metals were determined using a Fourier-transform infrared spectroscope (FT-IR-200, JASCO, Japan). The number of oxygen-containing functional groups in ACF was quantitatively determined using Boehm titration [50].

3.4. Experimental Procedure

The simultaneous removal of SO_3^{2-} and heavy metals (Hg^{2+}, Cd^{2+}, and Ni^{2+}) was conducted in a bubbling reactor with a gas flow rate of 1 L/min. The pure nitrogen and oxygen were blended

at different ratio by the mass flowmeters and injected into the reactor as oxidation gas. A typical adsorption-catalysis experiment was conducted with a stirring rate of 860 rpm at 45 °C for 2 h. In each run of this experiment, 10 g of $MgSO_3$, 40 μg of Hg^{2+}, and 0.4 g of 40% Co-ACFs were added to the reactor to obtain a total volume of 200 mL. The pH value of the solution was adjusted to be 6 with a 0.1 M NaOH or HCl solution. The reaction solution was filtered and measured at various intervals. The sulfate concentration was determined by conducting barium sulfate spectrophotometry [51] and the sulfite oxidation rate was obtained by plotting the sulfate concentration versus the reaction time in accordance with our previous study. The residual heavy metal ions in the solution were simultaneously measured using an atomic fluorescence spectrometer. The catalytic adsorption experiments of Cd^{2+} (2 mg/ L) and Ni^{2+} (10 mg/L) solutions were the same as aforementioned.

A typical kinetic experiment was conducted. In each run of this experiment, three 0.20 g of 40% Co-ACFs were added to 100 mL Hg^{2+} (2 mg/L), Cd^{2+} (2 mg/L), and Ni^{2+} (10 mg/L)) solutions in a temperature-controlled shaker. The pH was adjusted to 6 by using 1 M HCl and 1 M NaOH. The reaction was maintained at 45 °C for 2 h. After the reaction was terminated, the product was filtrated through a 0.22-mm microporous membrane. Then, the dissolved heavy metal ions remaining in the solution were measured.

3.5. Methodology

The adsorption capacity and removal efficiency of Co-ACFs for Hg^{2+}, Cd^{2+}, and Ni^{2+} were calculated as shown in Equations (2) and (3):

$$q_e = V(C_0 - C_e)/m \quad (2)$$

$$\eta = [C_0 - C_e)/C_0] \times 100\% \quad (3)$$

The Langmuir [52] and Freundlich [53] models, which are classical isothermal adsorption models, were used to determine the maximum adsorption capacity of Co-ACF for heavy metal ions. The maximum adsorption capacity obtained using Langmuir and Freundlich models can be expressed by Equations (4) and (5), respectively:

$$\frac{C_e}{q_e} = \frac{1}{q_m k_L} + \frac{C_e}{q_m} \quad (4)$$

$$\ln q_e = \ln k_F + \frac{1}{n_F} \ln C_e \quad (5)$$

Moreover, both pseudo-first-order [54] and pseudo-second-order [55] models were employed to simulate the adsorption processes of Hg^{2+}, Cd^{2+}, and Ni^{2+}. These models were described using Equations (6) and (7), respectively:

$$\ln(q_e - q_t) = \ln q_e - k_1 t \quad (6)$$

$$\frac{t}{q_t} = \frac{1}{K_2 q_e^2} + \frac{t}{q_e} \quad (7)$$

4. Conclusion

We have successfully synthesized Co-ACFs catalyst-adsorbent materials for the simultaneous catalytic oxidation of magnesium sulfite and the removal of Hg^{2+}, Cd^{2+}, and Ni^{2+} present in the magnesia flue gas desulfurization process. The experimental results revealed that the surfaces of ACFs pretreated with nitric acid contained a large number of oxygen-containing acidic groups. The oxidation rate of magnesium sulfite reached the maximum when the loading of cobalt is 40%, which was 5.69 times higher than the non-catalytic rate. In contrast, the catalytic oxidation rate of $MgSO_3$ approached five times the noncatalytic rate in the presence of heavy metal ions, indicating that the presence of heavy metal ions slightly inhibited the oxidation of magnesium sulfite. Moreover, the inhibition intensity was in the following order: $Ni^{2+} > Hg^{2+} > Cd^{2+}$.

The adsorption of Hg^{2+}, Cd^{2+}, and Ni^{2+} by Co-ACFs follows the pseudo-second-order kinetic model, which proved that the removal of heavy metals was controlled by the chemical adsorption process. The Langmuir model described the adsorption behavior of Hg^{2+}, Cd^{2+}, and Ni^{2+} by the Co-ACFs better than the Freundlich model, thus indicating that the adsorption of heavy metals is a monolayer adsorption process. The maximum adsorption capacities were calculated to be 333.3, 500, and 52.6 mg/g for Hg^{2+}, Cd^{2+}, and Ni^{2+}. The removal efficiency of Hg^{2+}, Cd^{2+}, and Ni^{2+} attained the maximum value at a pH value in the range from 5 to 6, which was consistent with the typical conditions of the desulfurization slurry. These results can be used as a reference for the simultaneous catalysis of sulfite oxidation and uptake of heavy metal ions by modified ACFs in the wet-desulfurization process.

In the industrial application, the Co-ACFs will be deposited and covered on the surface of support mold, such as cordierite, in order to facilitate its recovery and regeneration. After the prepared dual-functional material was enriched with heavy metals because of adsorption, it can be regenerated by either heating or elution. For instance, Co-ACFs can be immersed in the eluent of EDTA (ethylene diamine tetraacetic acid) for stripping the adsorbed heavy metals. Meanwhile, the active cobalt was reserved on the surface of ACFs due to their strong binding force, resulting in the regeneration of Co-ACFs catalyst.

Supplementary Materials: The following are available online at http://www.mdpi.com/2073-4344/10/2/244/s1. Figure S1: XPS spectrum of 40% Co-ACFs; Figure S2: Catalysis performance of Co-ACFs after four cycles; Figure S3: Comparison of the catalysis activity of Co based catalysts on magnesium sulfite oxidation at a concentration of 0.5 g/L. Table S1: Comparison of adsorption capacities for heavy metals onto different absorbents.

Author Contributions: Experiment: M.H. and Y.Y.; Data Curation: M.H. and Y.W.; Writing—Original Draft Preparation: Y.W. and T.Q.; Writing—Review and Editing: Y.W., T.Q., and L.W.; Software: Y.W. and L.X.; Supervision: L.W.; Funding Acquisition: L.W. All authors have read and agreed to the published version of the manuscript.

Funding: The present work is supported by the National Key Research and Development Program of China (No. 2016YFC0204102), the National Natural Science Foundation of China (No. 51878273), and the Natural Science Foundation of Hebei Province (No. E2019502199).

Acknowledgments: This manuscript was edited by Wallace Academic Editing.

Conflicts of Interest: The authors declare no conflict of interest.

Nomenclature

C_0	initial concentration of heavy metals in the solution (mg/L)
Ce	equilibrium concentration of heavy metals in the solution (mg/L)
V	solution volume (L)
m	mass of the catalytic-adsorbent (g)
η	removal efficiency (%)
q_e	adsorption capacity at equilibrium (mg/g)
q_m	maximum adsorption capacity of the adsorbent (mg/g)
k_L	Langmuir equilibrium adsorption constant (L/mg)
k_F	Freundlich empirical constant (mg/g)
n_F	Freundlich empirical constant (L/mg)
q_t	adsorption capacity at time t (mg/g)
k_1	equilibrium rate constant of the pseudo-first-order adsorption (min^{-1})
k_2	equilibrium rate constant of the pseudo-second-order adsorption (g/(mg.min))

References

1. Yuan, Y.; Zhang, J.; Li, H.; Li, Y.; Zhao, Y.; Zheng, C. Simultaneous removal of SO_2, NO and mercury using TiO_2-aluminum silicate fiber by photocatalysis. *Chem. Eng. J.* **2012**, *192*, 21–28. [CrossRef]
2. Ma, Y.; Qu, Z.; Xu, H.; Wang, W.; Yan, N. Investigation on mercury removal method from flue gas in the presence of sulfur dioxide. *J. Hazard. Mater.* **2014**, *279*, 289–295. [CrossRef] [PubMed]

3. Yang, J.; Zhao, Y.; Chang, L.; Zhang, J.; Zheng, C. Mercury Adsorption and Oxidation over Cobalt Oxide Loaded Magnetospheres Catalyst from Fly Ash in Oxyfuel Combustion Flue Gas. *Environ. Sci. Technol.* **2015**, *49*, 8210–8218. [CrossRef]
4. Liu, X.; Zhu, T.; Lv, Q.; Li, Y.; Che, D. Simultaneous removal of NO and SO_2 from coal-fired flue gas based on the catalytic decomposition of H_2O_2 over $Fe_2(MoO_4)_3$. *Chem. Eng. J.* **2019**, *371*, 486–499. [CrossRef]
5. Shen, Z.; Chen, X.; Tong, M.; Guo, S.; Ni, M.; Lu, J. Studies on magnesium-based wet flue gas desulfurization process with oxidation inhibition of the byproduct. *Fuel* **2013**, *105*, 578–584. [CrossRef]
6. Shen, Z.; Guo, S.; Kang, W.; Zeng, K.; Yin, M.; Tian, J.; Lu, J. Kinetics and Mechanism of Sulfite Oxidation in the Magnesium-Based Wet Flue Gas Desulfurization Process. *Ind. Eng. Chem. Res.* **2012**, *51*, 4192–4198. [CrossRef]
7. Li, Q.; Wang, L.; Zhao, Y.; Ma, Y.; Cui, S.; Liu, S.; Xu, P.; Hao, J. Oxidation Rate of Magnesium Sulfite Catalyzed by Cobalt Ions. *Environ. Sci. Technol.* **2014**, *48*, 4145–4152.
8. Barron, C.; O'Hern, H. Reaction kinetics of sodium sulfite oxidation by the Rapid-mixing method. *Chem. Eng. Sci.* **1966**, *21*, 397–404. [CrossRef]
9. Wang, Q.; Liu, Y.; Wang, H.; Weng, X.; Wu, Z. Mercury Re-emission Behaviors in Magnesium-Based Wet Flue Gas Desulfurization Process: The Effects of Oxidation Inhibitors. *Energy Fuels* **2015**, *29*, 2610–2615. [CrossRef]
10. Liu, Y.; Wang, Q.; Mei, R.; Wang, H.; Weng, X.; Wu, Z. Mercury re-emission in flue gas multipollutants simultaneous absorption system. *Environ. Sci. Technol.* **2014**, *48*, 14025–14030. [CrossRef]
11. Wang, Q.; Liu, Y.; Yang, Z.; Wang, H.; Weng, X.; Wang, Y.; Wu, Z. Study of mercury re-emission in a simulated WFGD solution containing thiocyanate and sulfide ions. *Fuel* **2014**, *134*, 588–594. [CrossRef]
12. Lidong, W.; Juan, W.; Peiyao, X.; Qiangwei, L.; Wendi, Z.; Shuai, C. Selectivity of transition metal catalysts in promoting the oxidation of solid sulfites in flue gas desulfurization. *Appl. Catal. A Gen.* **2015**, *508*, 52–60. [CrossRef]
13. Wang, L.; Qi, T.; Wu, S.; Zhang, S.; Qi, D.; Xiao, H. A green and robust solid catalyst facilitating the magnesium sulfite oxidation in the magnesia desulfurization process. *J. Mater. Chem. A* **2017**, *5*, 8018–8028. [CrossRef]
14. Wang, L.; Wu, S.; Liu, S.; Cui, S.; Liu, J.; Zhang, S. Cobalt impregnated porous catalyst promoting ammonium sulfate recovery in an ammonia-based desulfurization process. *Chem. Eng. J.* **2018**, *331*, 416–424. [CrossRef]
15. Li, M.; Qi, T.; Yang, R.; Xiao, H.-N.; Fang, Z.; Hodge, S.A.; James, T.D.; Wang, L.; Mao, B. Promoting magnesium sulfite oxidation via partly oxidized metal nanoparticles on graphitic carbon nitride (g-C_3N_4) in the magnesia desulfurization process. *J. Mater. Chem. A* **2018**, *6*, 11296–11305. [CrossRef]
16. Wang, L.; Qi, T.; Wang, J.; Zhang, S.; Xiao, H.; Ma, Y. Uniform dispersion of cobalt nanoparticles over nonporous TiO_2 with low activation energy for magnesium sulfate recovery in a novel magnesia-based desulfurization process. *J. Hazard. Mater.* **2018**, *342*, 579–588. [CrossRef]
17. Qi, T.; Wang, L.; Wang, Y.; Xing, L.; Zhang, L.; Liu, J.; Xiao, H.; Zhang, S. Suppressing Ammonia Re-Emission with the Aid of the Co3O4-NPs@KIT-6 Catalyst in Ammonia-Based Desulfurization. *Environ. Sci. Technol.* **2019**, *53*, 13477–13485. [CrossRef]
18. Li, M.; Guo, Q.; Xing, L.; Yang, L.; Qi, T.; Xu, P.; Zhang, S.; Wang, L. Cobalt-based metal-organic frameworks promoting magnesium sulfite oxidation with ultrahigh catalytic activity and stability. *J. Colloid Interface Sci.* **2020**, *559*, 88–95. [CrossRef]
19. Li, C.M.; Wang, X.P.; Jiao, Z.H.; Zhang, Y.S.; Yin, X.B.; Cui, X.M.; Wei, Y.Z. Functionalized Porous Silica-Based Nano/Micro Particles for Environmental Remediation of Hazard Ions. *Nanomaterials* **2019**, *9*, 247. [CrossRef]
20. Subramaniam, M.N.; Goh, P.S.; Lau, W.J.; Ismail, A.F. The Roles of Nanomaterials in Conventional and Emerging Technologies for Heavy Metal Removal: A State-of-the-Art Review. *Nanomaterials* **2019**, *9*, 625. [CrossRef]
21. Pan, L.; Wang, Z.; Yang, Q.; Huang, R. Efficient Removal of Lead, Copper and Cadmium Ions from Water by a Porous Calcium Alginate/Graphene Oxide Composite Aerogel. *Nanomaterials* **2018**, *8*, 957. [CrossRef] [PubMed]
22. Chowdhury, T.; Zhang, L.; Zhang, J.; Aggarwal, S. Removal of Arsenic(III) from Aqueous Solution Using Metal Organic Framework-Graphene Oxide Nanocomposite. *Nanomaterials* **2018**, *8*, 1062. [CrossRef] [PubMed]

23. Tummino, M.L.; Testa, M.L.; Malandrino, M.; Gamberini, R.; Bianco Prevot, A.; Magnacca, G.; Laurenti, E. Green Waste-Derived Substances Immobilized on SBA-15 Silica: Surface Properties, Adsorbing and Photosensitizing Activities towards Organic and Inorganic Substrates. *Nanomaterials* **2019**, *9*, 162. [CrossRef] [PubMed]
24. Li, J.; Xing, X.; Li, J.; Shi, M.; Lin, A.; Xu, C.; Zheng, J.; Li, R. Preparation of thiol-functionalized activated carbon from sewage sludge with coal blending for heavy metal removal from contaminated water. *Environ. Pollut.* **2018**, *234*, 677–683. [CrossRef] [PubMed]
25. Bandaru, N.M.; Reta, N.; Dalal, H.; Ellis, A.V.; Shapter, J.; Voelcker, N.H. Enhanced adsorption of mercury ions on thiol derivatized single wall carbon nanotubes. *J. Hazard. Mater.* **2013**, *261*, 534–541. [CrossRef]
26. Wang, Y.; Ye, G.; Chen, H.; Hu, X.; Niu, Z.; Ma, S. Functionalized metal–organic framework as a new platform for efficient and selective removal of cadmium(ii) from aqueous solution. *J. Mater. Chem. A* **2015**, *3*, 15292–15298. [CrossRef]
27. Liu, D.; Deng, S.; Vakili, M.; Du, R.; Tao, L.; Sun, J.; Wang, B.; Huang, J.; Wang, Y.; Yu, G. Fast and high adsorption of Ni(II) on vermiculite-based nanoscale hydrated zirconium oxides. *Chem. Eng. J.* **2019**, *360*, 1150–1157. [CrossRef]
28. Calderon, J.C.; Rios Rafales, M.; Nieto-Monge, M.J.; Pardo, J.I.; Moliner, R.; Lazaro, M.J. Oxidation of CO and Methanol on Pd-Ni Catalysts Supported on Different Chemically-Treated Carbon Nanofibers. *Nanomaterials* **2016**, *6*, 187. [CrossRef]
29. Wang, Y.; Tao, H.; Yu, D.; Chang, C. Performance Assessment of Ordered Porous Electrospun Honeycomb Fibers for the Removal of Atmospheric Polar Volatile Organic Compounds. *Nanomaterials* **2018**, *8*, 350. [CrossRef]
30. Yu, J.; Chi, C.; Zhu, B.; Qiao, K.; Cai, X.; Cheng, Y.; Yan, S. High adsorptivity and recycling performance activated carbon fibers for Cu(II) adsorption. *Sci. Total. Environ.* **2019**, *700*, 134412. [CrossRef]
31. Mena Aguilar, K.M.; Amano, Y.; Machida, M. Ammonium persulfate oxidized activated carbon fiber as a high capacity adsorbent for aqueous Pb(II). *J. Environ. Chem. Eng.* **2016**, *4*, 4644–4652. [CrossRef]
32. Huang, C.C.; Su, Y.J. Removal of copper ions from wastewater by adsorption/electrosorption on modified activated carbon cloths. *J. Hazard. Mater.* **2010**, *175*, 477–483. [CrossRef] [PubMed]
33. Lin, K.A.; Yang, M.T.; Lin, J.T.; Du, Y. Cobalt ferrite nanoparticles supported on electrospun carbon fiber as a magnetic heterogeneous catalyst for activating peroxymonosulfate. *Chemosphere* **2018**, *208*, 502–511. [CrossRef] [PubMed]
34. Beswick, O.; Yuranov, I.; Alexander, D.T.L.; Kiwi-Minsker, L. Iron oxide nanoparticles supported on activated carbon fibers catalyze chemoselective reduction of nitroarenes under mild conditions. *Catal. Today* **2015**, *249*, 45–51. [CrossRef]
35. Hung, C.M. Activity of Cu-activated carbon fiber catalyst in wet oxidation of ammonia solution. *J. Hazard. Mater.* **2009**, *166*, 1314–1320. [CrossRef]
36. Pradhan, B.; Sandle, N.K. Effect of Different Oxidizing Agent Treatments on the Surface Properties of Activated Carbons. *Carbon* **1999**, *37*, 1323–1332. [CrossRef]
37. Terzyk, A. The influence of activated carbon surface chemical composition on the adsorption of acetaminophen (paracetamol) in vitro: Part II. TG, FTIR, and XPS analysis of carbons and the temperature dependence of adsorption kinetics at the neutral pH. *Colloid Surf. A* **2001**, *177*, 23–45. [CrossRef]
38. Moreno-Castilla, C.; Lopez Ramon, M.V.; Carrasco-Marín, F. Changes in surface chemistry of activated carbons by wet oxidation. *Carbon* **2000**, *38*, 1995–2001. [CrossRef]
39. Castro, E.B.; Gervasi, C.A. Electrodeposited Ni–Co-oxide electrodes:characterization and kinetics of the oxygen evolution reaction. *Int. J. Hydrog. Energy* **2000**, *25*, 1163–1170. [CrossRef]
40. Taghavimoghaddam, J.; Knowles, G.P.; Chaffee, A.L. SBA-15 supported cobalt oxide species: Synthesis, morphology and catalytic oxidation of cyclohexanol using TBHP. *J. Mol. Catal. A Chem.* **2013**, *379*, 277–286. [CrossRef]
41. Zhang, F.; Zhang, S.; Guan, N.; Schreier, E.; Richter, M.; Eckelt, R.; Fricke, R. NO SCR with propane and propene on Co-based alumina catalysts prepared by co-precipitation. *Appl. Catal. B Environ.* **2007**, *73*, 209–219. [CrossRef]
42. Jia, C.J.; Schwickardi, M.; Weidenthaler, C.; Schmidt, W.; Korhonen, S.; Weckhuysen, B.M.; Schuth, F. Co_3O_4-SiO_2 nanocomposite: A very active catalyst for CO oxidation with unusual catalytic behavior. *J. Am. Chem. Soc.* **2011**, *133*, 11279–11288. [CrossRef] [PubMed]

43. Varga, E.; Ferencz, Z.; Oszkó, A.; Erdőhelyi, A.; Kiss, J. Oxidation states of active catalytic centers in ethanol steam reforming reaction on ceria based Rh promoted Co catalysts: An XPS study. *J. Mol. Catal. A Chem.* **2015**, *397*, 127–133. [CrossRef]
44. Sexton, B.A.; Hughes, A.E.; Turney, T. An XPS and TPR study of the reduction of promoted cobalt-kieselguhr Fischer-Tropsch catalysts. *J. Catal.* **1986**, *97*, 390–406. [CrossRef]
45. Li, Q.; Yang, Y.; Wang, L.; Xu, P.; Han, Y. Mechanism and kinetics of magnesium sulfite oxidation catalyzed by multiwalled carbon nanotube. *Appl. Catal. B Environ.* **2017**, *203*, 851–858. [CrossRef]
46. Wang, L.; Qi, T.; Hu, M.; Zhang, S.; Xu, P.; Qi, D.; Wu, S.; Xiao, H. Inhibiting Mercury Re-emission and Enhancing Magnesia Recovery by Cobalt-Loaded Carbon Nanotubes in a Novel Magnesia Desulfurization Process. *Environ. Sci. Technol.* **2017**, *51*, 11346–11353. [CrossRef]
47. Sathyamurthy, N.; Degaleesan, T.; Chandrasekharan, K.; Laddha, G. Absorption of oxygen by aqueous sodium sulphite solutions. *Can. J. Chem. Eng.* **1979**, *57*, 145–149. [CrossRef]
48. Li, J.; Liu, Y.; Ai, Y.; Alsaedi, A.; Hayat, T.; Wang, X. Combined experimental and theoretical investigation on selective removal of mercury ions by metal organic frameworks modified with thiol groups. *Chem. Eng. J.* **2018**, *354*, 790–801. [CrossRef]
49. Javadian, H.; Taghavi, M. Application of novel Polypyrrole/thiol-functionalized zeolite Beta/MCM-41 type mesoporous silica nanocomposite for adsorption of Hg^{2+} from aqueous solution and industrial wastewater: Kinetic, isotherm and thermodynamic studies. *Appl. Surf. Sci.* **2014**, *289*, 487–494. [CrossRef]
50. Boehm, H.P. Some Aspects of the Surface Chemistry of Carbon Black and Other Carbons. *Carbon* **1994**, *32*, 759–769. [CrossRef]
51. Lidong, W.; Shuai, C.; Qiangwei, L.; Juan, W.; Shuang, L. Kinetics and mechanism of magnesium sulphite oxidation promoted by a novel cobalt-based molecular sieve catalyst. *Appl. Catal. A Gen.* **2016**, *511*, 16–22. [CrossRef]
52. Kundu, S.; Gupta, A.K. Arsenic adsorption onto iron oxide-coated cement (IOCC): Regression analysis of equilibrium data with several isotherm models and their optimization. *Chem. Eng. J.* **2006**, *122*, 93–106. [CrossRef]
53. Pan, Y.; Wang, F.; Wei, T.; Zhang, C.; Xiao, H. Hydrophobic modification of bagasse cellulose fibers with cationic latex: Adsorption kinetics and mechanism. *Chem. Eng. J.* **2016**, *302*, 33–43. [CrossRef]
54. Ahmed, M.; Theydan, S. Equilibrium isotherms and kinetics modeling of methylene blue adsorption on agricultural wastes-based activated carbons. *Fluid Phase Equilib.* **2012**, *317*, 9–14. [CrossRef]
55. Ho, Y.-S.; McKay, G. Pseudo-Second Order Model for Sorption Process. *Process Biochem.* **1999**, *34*, 451–465. [CrossRef]